

# Multi-interactive Encoder-decoder Network for RGBT Salient Object Detection

Zhengzheng Tu, Zhun Li, Chenglong Li, Yang Lang, and Jin Tang

School of Computer Science and Technology, Anhui University, Hefei 230601, China

**Abstract.** RGBT salient object detection (SOD) aims to segment the common prominent regions by exploring and exploiting the complementary information of visible and thermal infrared images. However, existing methods simply integrate features of these two modalities, and thus could not explore the potentials of their complementarity. In this paper, we propose a novel multi-interactive encoder-decoder network to achieve an elaborative fusion for RGBT SOD. Our network relies on an encoder-decoder for the feature extraction and fusion, and we design a multi-interaction block (MIB) to model the interactions of different modalities, different layers and local-global information. In particular, we interact and integrate the multi-level features of different modalities in a two-stream decoder, which could fuse modal information sufficiently while maintaining their own specific feature representations for more robust detection performance. Moreover, each MIB block accepts both information from previous MIB and global context to restore more spatial details and object semantics respectively. Extensive experiments on the existing RGBT SOD datasets show that the proposed method achieves outstanding performance against the state-of-the-art algorithms.

## 1 Introduction

Salient object detection (SOD) aims at estimating the most conspicuous objects or regions in an image, which has been widely applied to many computer vision tasks [23,5]. Although being extensively studied, most of SOD algorithms cant perform well while dealing with the challenges in adverse environments, such as fog, haze, low illumination, etc, as RGB image catches deficient or equivocal semantic information in these cases.

Thermal infrared imaging could conquer the above challenges well, and it has shown its usefulness in SOD task [16,14,15]. Wang et al. [16] construct the first visible and thermal infrared (RGBT) SOD dataset called VT821 and propose a multi-task manifold ranking algorithm, which introduces a weight for each modality to describe the reliability and then adaptively fuses two modality with these weights. Tu et al. [14] use multi-modal multi-scale manifold ranking to achieve the fusion of different features. Further, Tu et al. [15] propose a collaborative graph learning algorithm to integrate the features extracted by fully convolutional network (FCN) [10], and also build a more standardized dataset called VT1000.

Although the above works promote the development of RGBT SOD to some extent, their performance is still limited, mainly caused by weak feature representation and excessive reliance on the results of superpixel segmentation. As we know, the handcraft features have great limitations on representing semantic relevance between pixels, and the superpixel-based methods require robust superpixel segmentation algorithm, but few of which can obtain steady good performances on various challenges. Therefore, our approach relies on an end-to-end trained FCN. Different from SOD in RGB images, how to take advantage of RGB and thermal information sufficiently is an important problem to be considered in RGBT SOD. Considering the imaging conditions in RGBT SOD, there are three situations described as following. (1) Both RGB and thermal infrared images contain the complete useful information for detecting the salient object; (2) Both RGB and thermal infrared images contain partial yet complementary useful information; (3) Only one modality contains useful information and another contains nothing for detecting the salient object. However, existing methods [16,14,15] simply integrate features of two modalities, and thus could not explore the potentials of their complementarity.

To handle the above problems, in this paper, we propose multi-interactive encoder-decoder network with a two-stream decoder to aggregate multilevel features for robust RGBT SOD. In particular, we design a multi-interaction block (MIB) to model the interactions of various information in fusion, and integrate the MIB in an encoder-decoder in a cascade manner. Each MIB receives four inputs including the encoded features of one modality, the outputs of previous MIB from two encoder paths and the global context information. On one hand, each MIB integrates the information of both modalities to perform cross-modality interactions. Such design could propagate the complementary useful features between modalities while maintaining the specific feature representations of each modality. On the other hand, each MIB block accepts both information from previous MIB (i.e., multilevel interactions) and global context (i.e., local-global interactions) to restore more spatial details and object semantics respectively. The global context is computed by incorporating the deepest encoded features of two modalities with pyramid pooling structure for various receptive fields, which contains strong semantic relevance of pixels within and between modalities. The global information is helpful for locating the object, and we thus fuse the global information in every MIB for improve the stable localization of salient objects.

All above three interactions could retain a sufficient fusion of different modalities and thus improve the performance clearly. In addition, we observe that existing RGBT SOD datasets have limited data to support the training of a robust pixel-wise detection network. To address this problem, we use an existing SOD dataset to train a CycleGan [26] for generating the corresponding synthetic thermal infrared images for data augmentation.

The contributions of this paper are summarized as follows. First, we propose a novel end-to-end trained deep encoder-decoder network to address the problem of sufficient fusion in RGBT SOD. Second, we design an effective multi-interaction block (MIB) to fuse the features of different modalities, different layers and

local-global information and integrate it into the encoder-decoder network in a cascaded way. Third, we design a data augmentation method by generating a large amount of synthetic training data using the generative adversarial network. Finally, experimental results demonstrate that the proposed method achieves a clear state-of-the-art performance against the existing methods on two public RGBT SOD datasets.

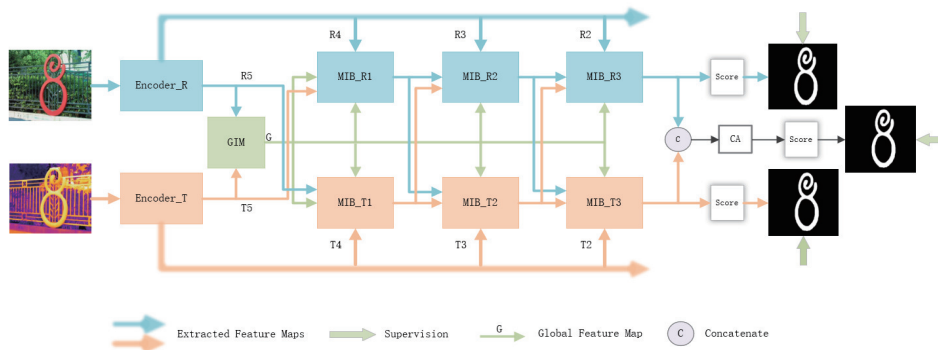


Fig. 1. The framework of our proposed method.

## 2 Related Work

**RGB Salient Object Detection.** In recent years, deep learning-based methods have achieved great progress in salient object detection. Wang et al. [17] utilize the neural network to perform the fusion of local spatial features and global semantic features, then combine local estimation with global search to predict saliency map. Liu et al. [8] design a deep hierarchical network to predict a coarse saliency map and then refine it hierarchically and progressively. Next, many researches come out based on fully convolutional network with its successful applications in semantic segmentation. Wang et al. [18] propose a recurrent FCN to constantly refine the saliency. Liu et al. [9] propose a novel pixel-level context-aware network that learns to pay selective attention to the context information of each pixel. Deng et al. [4] propose a module to learn the residual between the intermediate saliency prediction and the ground truth by alternatively using the low-level features and the high-level features. Wu et al. [21] design a cascaded partial decoder for fast and accurate salient object detection. Zhao et al. [24] introduce edge detection to SOD for more accurate boundaries. Numerous studies have made SOD algorithms more robust. However, with existing algorithms, it is difficult to deal with some challenges such as bad imaging conditions, which may cause defects or semantic ambiguity in visible images.

**RGBT Salient Object Detection.** With the availability of thermal sensors, many works [6,19] introduce the thermal infrared images to visible images as the complementary information. RGBT SOD are also gaining increasing attention. As the original work, Wang et al. [16] construct the first RGBT SOD dataset and propose a multi-task manifold ranking algorithm. Later, Tu et al. [14] use a multi-modal multi-scale manifold ranking to achieve the fusion of different features and introduce an intermediate variable to infer the optimal ranking seeds. Furthermore, Tu et al. [15] propose a collaborative graph learning method for RGBT SOD, which takes the superpixel as the graph node and uses hierarchical deep features to learn the graph affinity and node saliency. In addition, Tu et al. [15] also construct a larger RGBT SOD dataset. These RGBT SOD methods use traditional machine learning technologies, whereas we propose an end-to-end deep learning based method for RGBT SOD in this paper.

**Modality Fusion.** The existing RGBD SOD methods have explored some fusion strategies. Qu et al. [12] design the handcraft feature of input images, which is then used as the input of the network to predict the saliency map. Liu et al. [7] achieve fusion during the decoding phase by directly adding the features of two modalities with the feature from the previous decoding step. Instead of directly adding together, Chen et al. [1] design a novel complementarity-aware fusion module to fuse the features of two modalities. Later, Chen et al. [2] further propose a three-stream attention-aware network, in which a fusion stream is introduced that accompanies RGB-specific stream and depth-specific steam to extract the new fused features for each layer, then the fused features are used for decoding. The above-mentioned methods focus on how to combine the features of two modalities to obtain effective feature representations, which inevitably leads to information loss of some specific modality. Therefore, we propose a network with two-stream decoder, based on the original features of the two modalities to maintain the speciality of every modality.

### 3 The Propose Method

In this paper, we present multi-interactive encoder-decoder network for RGBT salient object detection. As shown in Fig. 1, we use two independent backbones to extract features from the visible images and thermal infrared images respectively. Then the global information module (GIM) is used to combine the high-level features of two modalities to obtain the global features with various receptive fields. In the decoding phase, we adopt a two-stream decoder based on two modalities and design the multi-interaction block (MIB) in a cascade way to sufficiently fuse different source data. Finally, we fuse the final features of the two decoders to predict the final saliency map. Details of each part are covered in the following subsections.

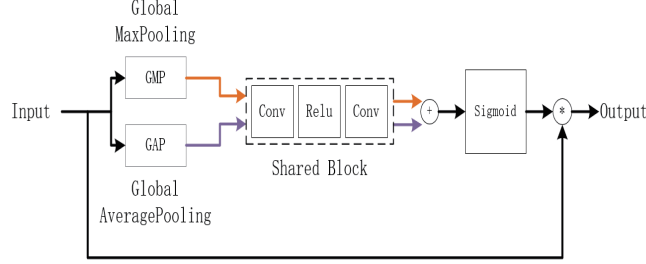


Fig. 2. Network structure of the channel attention.

### 3.1 Encoder Block

We use VGG16 [13] without the last pooling layer and two fully connected layers as our encoder to extract five features with different resolutions from the images of two modalities. As we know, the deeper layers encode high-level semantic information while the shallower layers contain more spatial details. The resolution of features from the first block is the same as the input image, and these features thus have a high computational complexity. To improve the efficiency, we abandon these high-resolution features of two modalities. For convenience, the remaining features extracted from the visible image are denoted as  $R_2 \sim R_5$  and those from thermal infrared image are denoted as  $T_2 \sim T_5$ .

### 3.2 Multi-Interaction Block

Different from merging two modalities' features during encoding or after encoding, we perform feature fusion in decoding phase. We adopt a two-stream decoder based on two modalities and design the multi-interaction block (MIB) in a cascade way to form the decoder, which can achieve the interactions between layers, modalities and global-local information. Benefiting from this structure, our network can make the utmost of two modalities for SOD. In details, as shown in Fig. 1, we use three MIBs in each decoder path to achieve interactions among various features. For clarity, these modules in decoding steps based on visible image are denoted as  $MIB_{R1\sim3}$ , and the corresponding three modules are denoted as  $MIB_{T1\sim3}$ . We use  $MIB_{R2}$  as an example and Fig. 3 shows the details of  $MIB_{R2}$ .

**Interactions in Multilevel Features** In each decoder path, we use the encoded features to restore the spatial details step by step and maintain the speciality of the corresponding modality. In  $MIB_{R2}$ ,  $R_3$  is used. We use the channel

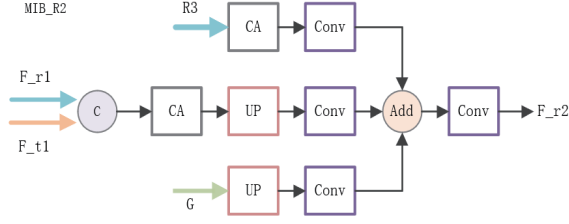


**Fig. 3.** Network structure of multi-interaction block.

attention to select more useful features for reconstruction, and then decrease the number of channels to 128.

$$\tilde{R}_3 = Conv(CA(R_3))$$

Where  $CA(*)$  is a simple channel-wise attention mechanism similar to CBAM [20] shown in Fig. 2 and the  $Conv(*)$  is a convolutional block, containing a convolutional layer, a batch normalize layer and a Relu function.

**Interactions between Modalities** For the interactions in two modalities, we concatenate the previous MIB outputs from two decoder paths. These output features contain previous fused information and the specific information of two modalities. In the top-down path, they are used as high-level semantic features with strong relevance in pixels. In  $MIB_{R2}$ , We first concatenate  $F_{r1}$  and  $F_{t1}$ , and then use the channel attention to achieve adaptive selection and reconstruction of the concatenated features. We up-sample the reconstructed features to the same size of  $R3$  and a convolutional block is applied to reduce the number of channels to 128. Thus, we have  $F_c$ .

$$\tilde{F}_c = Conv(UP(CA([F_{r1}, F_{t1}])))$$

where  $[*]$  is the channel-wise concatenation.

**Interactions of Local-global Information** In the top-down path, with the fusion of the spatial details, the location information of the object will be gradually diluted. Besides, although the high-level encoded features model the semantic relevance in pixels, the receptive field of VGG16 is too small so that the network cannot obtain sufficient semantic information, which might lead to missing some parts of big object or multiple objects. To handle these problems, we design the global information module (GIM). At first,  $R_5$  and  $T_5$  are simply aggregated, and then a channel attention mechanism is used to select more effective features. We use a convolutional block to decrease the channel number to 256, and the output is marked as  $F$ :

$$F = Conv(CA([R_5, T_5]))$$

Then four adaptive global max pooling operations with different sizes are used to obtain four feature maps with different receptive fields. We use four convolutional layers to reconstruct four feature maps respectively. After that, we up-sample all the four feature maps to the size of  $F$  and then concatenate them with  $F$ . Finally, we apply a convolutional layer to the concatenated features and generate the reconstructed features  $G$  which contains the information from global receptive field. The structure is shown as Fig. 4.

$$\tilde{F}_i = UP(Conv(MP_n(F)))$$

$$G = Conv([\tilde{F}_i]), i = 1, \dots, 4$$

where  $UP(*)$  is the up-sample operation and  $MP_n(*)$  is an adaptive max pooling with  $n * n$  output size.  $\tilde{F}_i$  represents the  $i$ -th branch's output where  $i = 1, 2, 3, 4$  with  $n = 1, 5, 9, 13$  respectively.

We add  $G$  into each MIB to maintain the stability of location. In  $MIB_{R2}$ , we up-sample  $G$  to the size of  $R_3$  and decrease the number of channels to 128:

$$\tilde{G} = Conv(UP(G))$$

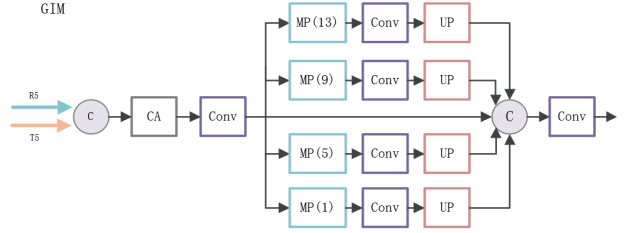


**Fig. 4.** Network structure of global information module.

**Integration of Various Features** We sum above three features directly and obtain the reconstructed fusion features  $F_{7,2}$  through a convolutional block as the output of  $MIB_{R2}$ :

$$F_{7,2} = Conv(\tilde{F}_c + \tilde{G} + \tilde{R}_3)$$

Other MIBs have the same operation except for different inputs. It should be noted that the interactions between two modalities only perform on the outputs of previous MIBs in two paths, and we still use the original features of the two modalities to obtain the low-level spatial details. Therefore, the final features from both decoders can effectively maintain the characteristics of the corresponding modality to some extent and also contain valid information. During three decoder steps, the interactions between hierarchical features, modalities

and the global information can be performed well, and the resolution of the last MIB’s output will be restored to 1/4 of the size of network input.

Finally, we fuse the final features ( $F_{r3}$  and  $F_{t3}$ ) from the two decoders by an concatenation operation and a simple channel-wise attention to predict the final saliency map. And then we up-sample the saliency map with the factor of 4 to the same size of the input image, marked as  $S_f$ .

### 3.3 Loss Function

Given the predicted saliency  $S = \{S_i | i = 1, \dots, T\}$  and the corresponding ground truth  $Y = \{Y_i | i = 1, \dots, T\}$ , where  $T$  is number of total pixels, the binary cross entropy loss commonly used in SOD task is formulated as follows:

$$L(S, Y) = - \sum_{i=1}^T (Y_i * \log(S_i) + (1 - Y_i) * \log(1 - S_i))$$

We predict two saliency maps for  $F_{r3}$  and  $F_{t3}$  denoted as  $S_1$  and  $S_2$ , and then compute the BCE loss with the ground truth  $Y$ :

$$L_d = L(S_1, Y) + L(S_2, Y)$$

Global semantic information plays an important role in the decoding stage, which directly affect the accuracy of salient object location. To make the GIM module be learned better, we predict a saliency map  $S_g$  from the global semantic features  $G$ . For the same size, we down-sample  $Y$  with the factor of 16 to obtain  $Y_g$ . Then, a BCE loss is used:

$$L_g = - \sum_{i=1}^{T_g} (Y_{gi} * \log(S_{gi}) + (1 - Y_{gi}) * \log(1 - S_{gi}))$$

where the  $T_g$  is the number of total pixels of  $S_g$ . For the final predicted map  $S_f$ , the loss function is:

$$L_f = L(S_f, Y)$$

Therefore, our total loss is:

$$L = L_d + L_g + L_f$$

## 4 Experiment

### 4.1 Dataset

VT821[16] contains 821 registered image pairs. To heighten the challenge of the dataset, the authors add noise to some visible images in VT821. The image pairs in VT821 are not aligned and need to be registered manually, so there are vacant regions existing in the thermal infrared images. In addition, some thermal infrared images are generated with different pseudo-color imaging modes.



VT1000[15] contains 1000 registered image pairs, with relatively simple scenes and well aligned images. So we choose VT1000 as the training set and VT821 as testing set.

As SOD is a visual task with pixel-level prediction, it is difficult to train a robust network with little data. Therefore, we use the CycleGan[26] to generate corresponding thermal infrared images of visible images. Since the synthesized data comes from the visible images, we think that the synthesized data should not be too much otherwise the network may learn some biased knowledge. Taking these factors into consideration, we choose a dataset ESSCD[22] to generate the synthesized data, as ESSCD contains 1000 visible images with annotations. Therefore, our training set is a collection of VT1000, ESSCD and its corresponding synthetic data.

## 4.2 Experimental Setup

**Implementation Details.** Our network is implemented based on Pytorch and trained with a single Titan Xp GPU. We use the stochastic gradient descent(SGD) to optimize parameters with the weight decay of 5e-4 and the momentum of 0.9. We train 20 epochs with batchsize of 4. The initial learning rate is 1e-3, and it becomes 1e-4 at the 11-th epoch and 1e-5 at the 16-th epoch. For the input, we resize all the images to the size of 400 \* 400 and use random horizontal flip for data enhancement. We just spend 150 minutes for the complete training.

**Evaluation metrics.** For evaluating the methods, we use precision-recall(PR) curve, F-measure and mean absolute error(MAE). The formula is expressed as follows:

$$F_{\beta} = \frac{(1 + \beta^2) \cdot Precision \cdot Recall}{\beta^2 \cdot Precision + Recall}$$

$$MAE = \frac{1}{T} \sum_{i=1}^T |S_i - Y_i|$$

Where  $\beta^2 = 0.3$  emphasizes the importance of precision.

## 4.3 Comparison with State-of-the-Art Methods

We compare our method with nine existing methods. They are SDGL[15], MTMR[16], DMRA[11], CDCP[25], R3Net[4], PiCANet[9], CPD[21], EGNet[24] and GCPANet[3]. SDGL and MTMR are existing RGB-T SOD methods. DMRA is the latest deep learning-based RGB-D SOD method and CDCP is a traditional method for RGB-D SOD. The other five methods are recent remarkable SOD methods. For fairness, we train all the deep learning-based methods on our training set. All methods are tested on VT821, and then we make statistics and analysis based on the results.

**Quantitative Evaluation.** Table 1 shows the results of our method and the

**Table 1.** Performance comparison with 9 state-of-the-art methods on VT821. The best results are highlighted in **boldface**.

Method	maxF	MAE
Our	<b>0.860</b>	0.0548
SDGL	0.780	0.0849
MTMR	0.747	0.1083
DMRA	0.840	0.0501
CDCP	0.680	0.1148
R3Net	0.783	0.0641
PiCANet	0.781	0.0835
CPD	0.832	0.0510
EGNet	0.819	<b>0.0419</b>
GCPANet	0.836	0.0624

other eight methods on VT821. It can be seen that our method outperforms against the existing two RGBT SOD methods with a large gap. This is mainly caused by the advantage of feature representation of deep network, and the semantic relevance between pixels is learnt well. Secondly, for two methods based on RGBD SOD, we explore the effectiveness of their modality fusion strategies on RGBT data. Both of CDCP and DMRA show poor performances on RGBT SOD task. Therefore, it can be seen that our multi-level interaction fusion structure is effective, and a further study for that is shown in the ablation experiment. Finally, we study the R3Net, PiCANet, CPD, EGNet and GCPANet, which have the most advanced performance on SOD. Since most of visible images have useful information, these methods also work well on VT821. Without the noise from the thermal infrared images, most of them show higher MAE. The PR curve of the ten methods on VT821 can be seen in Fig.6.

**Qualitative Evaluation.** The qualitative comparison can be seen in Fig.5. We can see our method outperforms the RGBT and RGBD SOD methods in the challengeable image pairs. Our network has considered the specialities of two modalities. Though one of the modality is useless, the other modality is rarely affected by the destructive information. When both of two modalities are informative, our network can take advantage of the complementarity of two modalities to gain more reliable relevance in pixels. Although the advanced SOD methods work well in informative visible images, they can't work well on the visible images with deficiency and semantic ambiguity.

#### 4.4 Ablation Analysis

In this section, we mainly study the effects of different configurations on network performance, as shown in Table 2. First, we study the supervision of the network. ' $L_d$  w/o' represents that we don't use the last features of the two decoders to

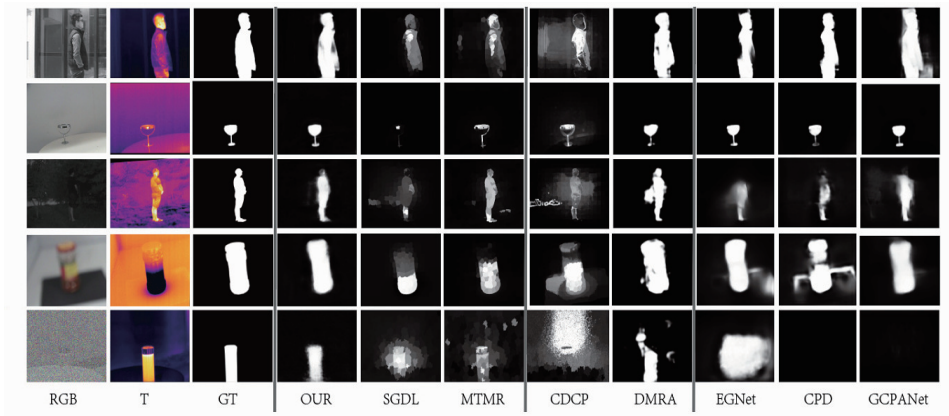


**Fig. 5.** Qualitative comparison of the proposed model with other methods.

calculate the saliency maps, and the supervision only exists in the final predicted saliency map. Similarly, the ' $L_g$  w/o' and ' $L_d, L_g$  w/o' disable the corresponding loss function. We can see that both of two loss function contribute a lot. Then, we discard the global information module(GIM w/o), the performance obviously declines, which indicates the importance of the interaction between global information and local information. In addition, in order to verify the effectiveness of two-stream decoding, we compare a single stream decoder structure that directly fuses the encoded features step by step. Without maintaining the specialities of two modalities, the ability to cope with various information distribution weakens. Finally, considering the effect of synthetic data on the experiment, we further compare the performance of training without synthetic data. The approximate 3% gains shows that the effectiveness of this kind of data augmentation.

**Table 2.** Ablation studies with different setup.

	maxF	MAE
baseline	<b>0.860</b>	<b>0.0548</b>
$L_d$ w/o	0.829	0.0669
$L_g$ w/o	0.834	0.0733
$L_d, L_g$ w/o	0.815	0.0868
GIM w/o	0.829	0.0684
SingleDecoder	0.824	0.0722
Synthesized Data w/o	0.827	0.0737

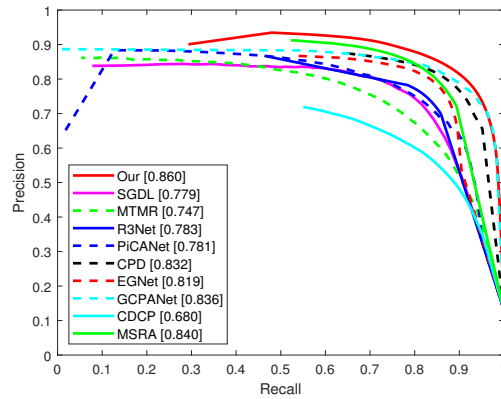


**Fig. 6.** The PR curve in the VT821 dataset.

## 5 Conclusion

In this paper, we propose a multi-interactive encoder-decoder network for RGBT SOD. Considering the different relevance among the encoded hierarchical features, modalities and local-global information, we design a two-stream decoder with cascaded MIBs to achieve multi-interaction step by step. Particularly, the proposed structure can prevent information of two modalities from excessive influence by each other during the interaction. Experimental results show the superiority of our method for RGBT SOD.

## References

1. Chen, H., Li, Y.: Progressively complementarity-aware fusion network for rgb-d salient object detection. In: Proceedings of the IEEE Conference on Computer Vision and Pattern Recognition. pp. 3051–3060 (2018)
2. Chen, H., Li, Y.: Three-stream attention-aware network for rgb-d salient object detection. *IEEE Transactions on Image Processing* **28**(6), 2825–2835 (2019)
3. Chen, Z., Xu, Q., Cong, R., Huang, Q.: Global context-aware progressive aggregation network for salient object detection (2019)
4. Deng, Z., Hu, X., Zhu, L., Xu, X., Qin, J., Han, G., Heng, P.A.: R3net: Recurrent residual refinement network for saliency detection. In: Proceedings of the 27th International Joint Conference on Artificial Intelligence. pp. 684–690. AAAI Press (2018)
5. Lee, H., Kim, D.: Salient region-based online object tracking. In: 2018 IEEE Winter Conference on Applications of Computer Vision (WACV). pp. 1170–1177. IEEE (2018)
6. Li, C., Zhu, C., Huang, Y., Tang, J., Wang, L.: Cross-modal ranking with soft consistency and noisy labels for robust rgb-t tracking. In: Proceedings of the European Conference on Computer Vision (ECCV). pp. 808–823 (2018)

7. Liu, D., Hu, Y., Zhang, K., Chen, Z.: Two-stream refinement network for rgb-d saliency detection. In: 2019 IEEE International Conference on Image Processing (ICIP). pp. 3925–3929. IEEE (2019)
8. Liu, N., Han, J.: Dhsnet: Deep hierarchical saliency network for salient object detection. In: Proceedings of the IEEE Conference on Computer Vision and Pattern Recognition. pp. 678–686 (2016)
9. Liu, N., Han, J., Yang, M.H.: Picanet: Learning pixel-wise contextual attention for saliency detection. In: Proceedings of the IEEE Conference on Computer Vision and Pattern Recognition. pp. 3089–3098 (2018)
10. Long, J., Shelhamer, E., Darrell, T.: Fully convolutional networks for semantic segmentation. In: Proceedings of the IEEE conference on computer vision and pattern recognition. pp. 3431–3440 (2015)
11. Piao, Y., Ji, W., Li, J., Zhang, M., Lu, H.: Depth-induced multi-scale recurrent attention network for saliency detection. In: Proceedings of the IEEE International Conference on Computer Vision. pp. 7254–7263 (2019)
12. Qu, L., He, S., Zhang, J., Tian, J., Tang, Y., Yang, Q.: Rgb-d salient object detection via deep fusion. IEEE Transactions on Image Processing **26**(5), 2274–2285 (2017)
13. Simonyan, K., Zisserman, A.: Very deep convolutional networks for large-scale image recognition. arXiv preprint arXiv:1409.1556 (2014)
14. Tu, Z., Xia, T., Li, C., Lu, Y., Tang, J.: M3s-nir: Multi-modal multi-scale noise-insensitive ranking for rgb-t saliency detection. In: 2019 IEEE Conference on Multimedia Information Processing and Retrieval (MIPR). pp. 141–146. IEEE (2019)
15. Tu, Z., Xia, T., Li, C., Wang, X., Ma, Y., Tang, J.: Rgb-t image saliency detection via collaborative graph learning. arXiv preprint arXiv:1905.06741 (2019)
16. Wang, G., Li, C., Ma, Y., Zheng, A., Tang, J., Luo, B.: Rgb-t saliency detection benchmark: Dataset, baselines, analysis and a novel approach. In: Chinese Conference on Image and Graphics Technologies. pp. 359–369. Springer (2018)
17. Wang, L., Lu, H., Ruan, X., Yang, M.H.: Deep networks for saliency detection via local estimation and global search. In: Proceedings of the IEEE Conference on Computer Vision and Pattern Recognition. pp. 3183–3192 (2015)
18. Wang, L., Wang, L., Lu, H., Zhang, P., Ruan, X.: Saliency detection with recurrent fully convolutional networks. In: European conference on computer vision. pp. 825–841. Springer (2016)
19. Wang, P., Bai, X.: Thermal infrared pedestrian segmentation based on conditional gan. IEEE transactions on image processing **28**(12), 6007–6021 (2019)
20. Woo, S., Park, J., Lee, J.Y., So Kweon, I.: Cbam: Convolutional block attention module. In: Proceedings of the European Conference on Computer Vision (ECCV). pp. 3–19 (2018)
21. Wu, Z., Su, L., Huang, Q.: Cascaded partial decoder for fast and accurate salient object detection. In: Proceedings of the IEEE Conference on Computer Vision and Pattern Recognition. pp. 3907–3916 (2019)
22. Yan, Q., Xu, L., Shi, J., Jia, J.: Hierarchical saliency detection. In: Proceedings of the IEEE Conference on Computer Vision and Pattern Recognition. pp. 1155–1162 (2013)
23. Zeng, Y., Zhuge, Y., Lu, H., Zhang, L.: Joint learning of saliency detection and weakly supervised semantic segmentation. In: Proceedings of the IEEE International Conference on Computer Vision. pp. 7223–7233 (2019)
24. Zhao, J.X., Liu, J.J., Fan, D.P., Cao, Y., Yang, J., Cheng, M.M.: Echnet: Edge guidance network for salient object detection. In: Proceedings of the IEEE International Conference on Computer Vision. pp. 8779–8788 (2019)

25. Zhu, C., Li, G., Wang, W., Wang, R.: An innovative salient object detection using center-dark channel prior. In: Proceedings of the IEEE International Conference on Computer Vision. pp. 1509–1515 (2017)
26. Zhu, J.Y., Park, T., Isola, P., Efros, A.A.: Unpaired image-to-image translation using cycle-consistent adversarial networks. In: Proceedings of the IEEE international conference on computer vision. pp. 2223–2232 (2017)